Double Hysteresis Loop and Loop Asymmetry in Perpendicularly Exchange-Biased Pt/Co/Pt/IrMn Thin Films

M. Öztürk*

Gebze Technical University, Department of Physics, 41400 Kocaeli, Turkey

Received: 16.01.2021 & Accepted: 20.05.2021

Doi: 10.12693/APhysPolA.140.20 *e-mail: mozturk@gtu.edu.tr

Double hysteresis loops and asymmetric reversals were observed for perpendicularly magnetized and exchange-biased Pt/Co/Pt/IrMn thin films in the magneto-optic Kerr effect and the Hall effect measurements. Drastic changes in double hysteresis loop and loop asymmetry were found in the magnetization reversal process of the Pt/Co/Pt/IrMn structures with the increase of antiferromagnet layer thickness. The applied external magnetic field angle was varied from easy axis to hard axis of magnetization, where changes in the asymmetry of hysteresis loops were observed. Reasons for the double hysteresis loops and asymmetric loops were discussed. The results of this study emphasize the importance of the antiferromagnetic film thickness and the applied magnetic field angle for the exchange-biased bilayers.

topics: asymmetric hysteresis loops, double hysteresis loops, exchange bias, perpendicular anisotropy

1. Introduction

The exchange bias (EB) effect is defined as a shift of the ferromagnetic hysteresis loop due to the interlayer exchange coupling when a ferromagnet (FM) and an antiferromagnet (AFM) are in close contact with each other [1]. Although many studies have been carried out related to this phenomenon in the last decades, research on different aspects of the EB effect is continued today due to its importance in many kinds of technological devices [2–5].

The EB effect mostly manifests itself as a negative or positive loop shift along the field axis when an exchange-biased sample is cooled through the Néel temperature of an AFM material to the measurement temperature under a proper magnetic field [4–9]. In some circumstances, double hysteresis loops (DHLs) in exchange-biased bilayers are also observed in [10–12]. One case for obtaining DHLs is the measurement of as-grown samples directly, without applying any kind of a cooling process [12]. Another well-known procedure for obtaining DHLs is to anneal the sample to a higher temperature above the Néel temperature of AFM and then cool it with zero field or under appropriate magnetic field before its hysteresis loop measurements [11, 12].

DHLs in the samples are generally linked to bidomain states with two opposite local EB effects [11, 13]. The bidomain state can originate either from FM domains or AFM domains separately [10, 12], or from the FM and AFM domains simultaneously [14]. In general, the size of the AFM domains shall be larger than the FM domains for DHLs to occur. Otherwise, DHLs are lost due to the average overall effect of interlayer exchange coupling caused by the small AFM domains [14].

Apart from the loop shifts, asymmetric behavior at the ascending and descending branches of the hysteresis loops can be observed in some exchange-biased samples as well [15–17]. The asymmetry of a hysteresis loop can be attributed to different kinds of mechanisms for a magnetic reversal of descending and ascending branches. In general, one branch is then referred to coherent rotation while the other part is referred to domain nucleation and domain wall (DW) motion [17–19]. In such studies, various causes are correlated as the origin of asymmetric hysteresis loops, e.g., the presence of higher-order anisotropies [19]; irreversibilities due to training effect [20]; noncollinearity of the FM and AFM anisotropy axes [17, 21]; inhomogeneity of the laterally structured samples [22]; the intrinsic properties with collinear anisotropies [23]. It is also found that the asymmetry can depend on the measurement angle, i.e., the reversal can be more symmetrical when the field is applied along the hard axis [18].

The occurrence of both the DHLs and the asymmetric reversals for perpendicularly exchange-biased samples is very rare in the literature. In this paper, DHLs are observed in the perpendicularly exchange-biased Pt/Co/Pt/IrMn thin films. Moreover, asymmetric reversal modes are found for the sample with a thick IrMn layer. Possible reasons of the occurrence of both the DHL and the loop

asymmetry, as well as their polar angle dependences, are discussed for this thick sample. The study sheds light on the understanding of both issues for a particular case of perpendicularly magnetized samples.

2. Materials and methods

Polycrystalline Pt(10 nm)/Co(0.6 nm)/Pt(0.6 nm) /IrMn(t_{IrMn}) thin films were deposited onto Si(100)/SiO_2(500 nm) substrates at room temperature without applying external magnetic field by using a magnetron sputter system. For simplicity, the samples in the article were named using their IrMn layer thicknesses as: IM0, IM10 and IM20, where $t_{\mathrm{IrMn}} = 0$, 10, and 20 nm, respectively. The first sample, namely IM0, has a capping layer of 3 nm Pt on its top to protect the Co layer from oxidation. Due to the skin depth region limitation of the laser beam, for samples with IrMn layers, no other capping layer was used for keeping the total thickness at a minimum for magnetic measurements. However, the lack of capping layers on top of IrMn layers may cause a thin oxidized layer at the surfaces and may reduce the effective thickness of IrMn, as was pointed out in the previous articles [24, 25]. In the samples, the FM Co layer has two adjacent Pt layers in order, so consequently the surface anisotropy terms become very important — as the Co layer is ultrathin — and increase the effective perpendicular magnetic anisotropy (PMA) [26, 27]. However, it shall be noted that the 0.6 nm Pt spacer layer can be also responsible for the decrease of the EB effect due to the short-range character of EB [26].

A 10 W DC generator for the growth of IrMn and Pt layers, and a 20 W RF generator for the growth of the Co layer were used in the sputtering system. The base and deposition pressures were kept in the order of 10^{-9} mbar and 10^{-3} mbar, respectively. These were the optimum values of the used sputtering system for the targets which were, prior to the study, determined by the structural and magnetic analysis of another sample set [28]. Nominal values of layer thickness, density and roughness parameters were checked with X-ray reflectivity (XRR) measurements. The XRR data and simulation results for the IM0 sample are given in Fig. 1, while the fitting parameters for the sample are shown in Table I. The calculated thickness values of the layers are very close to the nominal ones and the interfaces may be considered smooth due to the calculated roughness values. However, since the Co layer is ultra thin, thus possible effects of interface roughness on the magnetic properties such as reducing PMA [29] or causing lateral discontinuity [30] may occur. These are discussed along with magnetic measurements in Sect. 3. The roughness in the sample can be attributed to the interdiffusion of sputtered materials as all elements used in sputtered systems can form alloys [31, 32].

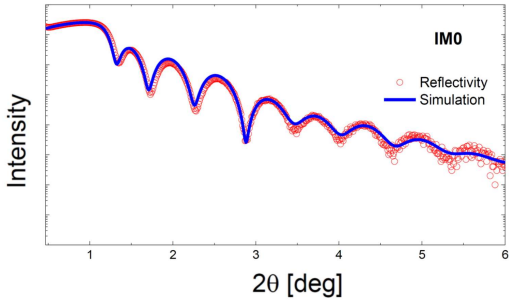

Fig. 1. Small angle X-ray reflectivity measurement and simulation data for the IM0 sample.

TABLE I
Fitting parameters for the IM0 sample.

Layer	Density [g/cm^3]	Thickness [nm]	Roughness [nm]
SiO_2	2.6	500	0.33
Pt	21.4	9.99	0.75
Co	8.9	0.57	0.82
Pt	21.4	2.98	0.71

The magnetic property measurements of the samples were carried out by using the magneto-optic Kerr effect (MOKE) [33] and anomalous Hall effect (HE) techniques [34]. The samples measured in this study were in the form of continuous thin films with surface dimensions of 1×1 cm^2. The front end of our MOKE system has a self-polarized HeNe laser operating at 632.8 nm (25LHP991230, Melles Griot) with a beam diameter of 0.65 mm. This small beam diameter relative to the sample sizes allows MOKE measurements to be taken from various surface regions of the continuous thin films when the consistency of measurements from different regions is required. For the Hall measurements, the 4-point Van der Pauw method was preferred. A DC current of 2 mA has been applied to the samples by using a current source (Keithley 6221). In turn, the Hall voltages have been recorded by using a nanovoltmeter (Keithley 2182) during HE measurements. All MOKE and HE measurements in the study were performed at room temperature in the as-grown state without any kind of cooling. In order to compare and assess the results obtained from both methods, we presented the normalized data.

3. Experiment and discussion

Figure 2a shows the normalized polar MOKE measurements of samples for the out-of-plane geometry at which the external magnetic field $\boldsymbol{H}$ is applied parallel to the film normal ($\theta_H = 0°$). At this easy axis, the sample without IrMn (IM0) has almost a perfect symmetrical square-shaped hysteresis curve, thus indicating a strong PMA. The other samples with IrMn (IM10 and IM20) also have perpendicular magnetization, but due to the

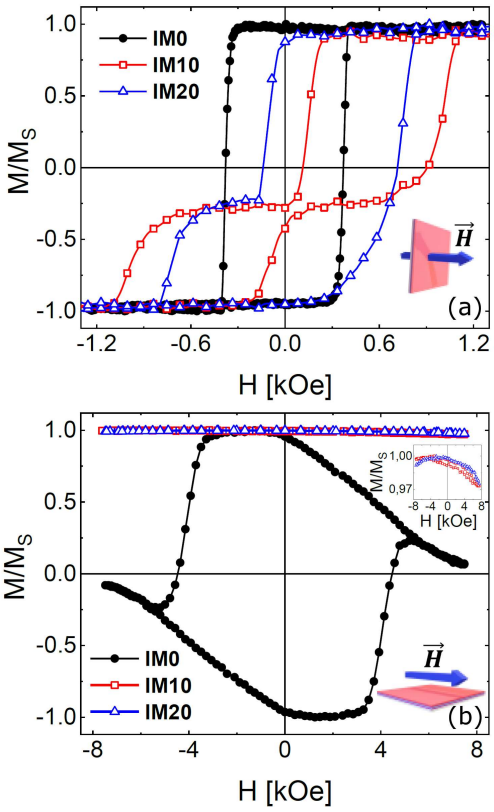

Fig. 2. MOKE measurements of IM0 (circles), IM10 (squares) and IM20 (triangles) (a) at the out-of-plane ($\theta_H = 0\circ$) and (b) at the in-plane geometries ($\theta_H \simeq 90°$). The inset of (b) focuses on IM10 and IM20 measurements to clearly demonstrate the arc-shaped behavior. Lines in the figures are provided as guides to the eye.

EB effect the step-like hysteresis curves occur there. This indicates that the interlayer exchange coupling of the uncompensated spins of Co and IrMn produces a bidomain state with both positive and negative perpendicular EB effects. Similar double shifts have been reported for the as-grown samples due to formation of large antiferromagnetic domains [12], where the value of the EB field (H_{EB}) and the shape of double shift have remained almost stable with the increase of IrMn thickness [12].

In this study, however, the IM20 sample demonstrated a slightly different behavior. Figure 2a shows that the change in the thickness of thin AFM layers has significant influence on the magnetization reversal process. The field values of the loop shift for IM20 seems to be decreasing as compared to the value of IM10, and the double shifted loop is not symmetric for IM20 at the out-of-plane. The step-like hysteresis behavior is only observed at the descending branch of the curve for IM20. This asymmetric one-sided step-like loop appears similar to the loops of the multilayered spin-valve structures [35, 36]. Yet, it is significant to point out that the structure in our study is not a spin valve, since it has only one FM layer.

Figure 2b shows the normalized in-plane MOKE results of the samples for the $\boldsymbol{H}$ parallel to the film plane ($\theta_H \simeq 90°$). At this hard axis, the coercive field values of IM0 increase, as compared to its out-of-plane easy axis values. In fact, the coercive field values are expected to increase in IM10 and IM20 samples as well. However, instead of a hysteresis behavior, the arc-shaped graphs are obtained for IM10 and IM20. This is probably caused by the magnetic field limitation of the MOKE measurement technique. The occurrence of the growth of the coercive field values for all samples with the rotation of the external magnetic field from the easy axis to the hard axis can be related to their strong PMA. Details of similar observations of the increase in the coercive field have been previously discussed in [28, 37].

To clarify the existence of the asymmetric behavior in the hysteresis loops of IM20, polar angle-dependent experiments were carried out. Since it is difficult to make the polar angle-dependent measurements with a MOKE setup, the HE technique was performed to these measurements. In the beginning, the asymmetric hysteresis behavior for IM20 should be verified by both techniques at easy axis with the step-like descending and stepless ascending branches. Both techniques are indirect methods of measuring the magnetic properties of materials. Hence, in addition to the practical advantage of HE, measurement consistency of both techniques can confirm that the asymmetry is neither a randomly encountered effect on the sample nor it is a technical artefact resulting from any measurement setup.

Polar angle-dependent magnetization curves are measured with the HE technique from $\theta_H = 0°$ to 180°. (Note that the azimuthal angle between the current and the magnetic field, φ_H, is always kept as zero.) The change in the external field angles provides a defined initial direction for the reversal process by canting magnetization from the perpendicular direction. Figure 3a and 3b show some of the HE measurements taken at significant angles ($\theta_H = 0°, 82°, 85°, 90°, 97°$, and 180°). The values of R_{Hall} [mΩ] are calculated by dividing the measured Hall voltage to the applied Hall current (2 mA). As shown in Fig. 3, with the polar angle growth from zero to 85°, the coercive fields increase as well and the left-sided step-like curves become two-sided and more symmetrical. At around the angle of 90°, the curve is arc-shaped (as obtained in the MOKE measurement shown in Fig. 2b). Above the 90° angle, since the relative directions of the applied magnetic fields with the sample are reversed, the shapes of the curves are also reversed — a consequence of mirror symmetry of the measurements below 90°. Therefore, regardless of the sample rotation, the bi-domain state is always present in the sample, however it becomes clearer with the increasing angle.

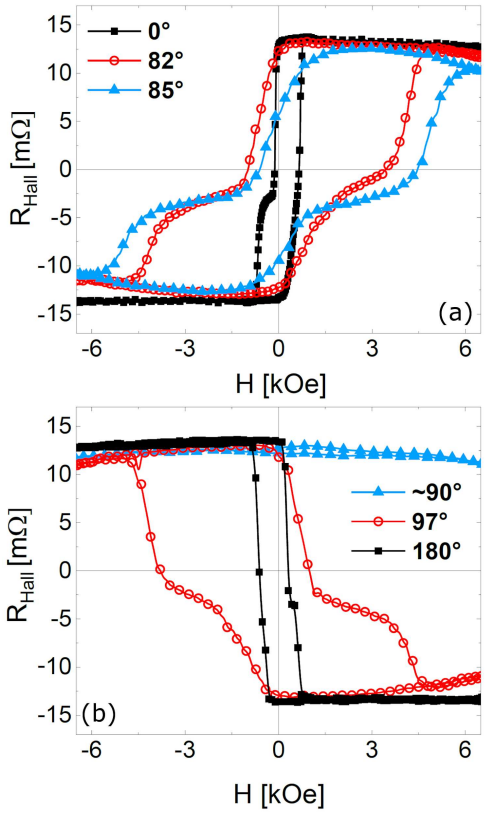

Fig. 3. The angle-dependent Hall measurement results for the IM20 sample (a) at $\theta_H = 0°$, 82° and 85° and (b) at $\theta_H = 90°$, 97° and 180°. Lines in the figures are provided as guides to the eye.

In order to understand possible reasons for the emergence of DHLs with an increasing polar angle, we examined the switching field values which can also be called the local coercive field values. The switching field dependences of IM20 are drawn in terms of increasing polar angles in Fig. 4. The upper inset of Fig. 4 is provided in order to clarify the definitions of switching field terms with symbols on a hysteresis loop taken at $\theta_H = 85°$. Notations of H_{S1u} and H_{S1l} are introduced for the upper and lower switching field values of the descending branches of the step-like hysteresis loops, respectively. Similarly, notations of H_{S2u} and H_{S2l} are devoted for the ascending branches. The lower insets in Fig. 4 show the Hall measurements taken at 20°, 60°, and 70°. The two-sided DHLs are clearer at 60° and 70° measurements. Obviously, the change of the direction of the applied magnetic field helps to enhance the visibility of DHLs for the angles close to the in-plane. In other words, the magnetization reversal starts to gain symmetry with the help of the in-plane projection of magnetic fields. The HE technique is known for measuring the perpendicular component of magnetization. Since the applied external magnetic field is in the film plane for the angles close to 90°, the measurements of perpendicular magnetization with the applied in-plane magnetic field prove a tendency of coherent rotation for magnetization at these angles. At hard axis direction (at $\theta_H = 90°$), the arc-shaped reversal loop appears to proceed entirely via a coherent rotation with the tilting of the magnetic moment vector and without any magnetization switching. This tilting describes a magnetization cycle without any discontinuity due to the strong PMA. On the other hand, the application of out-of-plane magnetic fields around easy axes ($\theta_H = 0°$ or 180°) causes different magnetization reversal modes and asymmetry. At these angles, the dominant magnetization reversal modes of IM20 in the backward branch can be related to the domain nucleation and DW propagation, while the dominant reversal modes in the forward one can be associated with coherent and partial rotations.

The occurrence of DHLs can be attributed to the EB effect of the bidomain state at the interface with the growth of the IrMn layer on top of Pt/Co/Pt thin films [12]. Apart from the DHLs, the samples have two other important properties as subjects of discussion in this article. One of the properties is the asymmetrical reversal loop in the IM20 sample and the other is the decrease of EB value with the increase of IrMn thickness for the IM0, IM10 and IM20 samples.

Magnetization reversals of magnetic materials with uniaxial anisotropy can take place either by rotations or by DW motions [18]. It is known that magnetization reversal occurs by the domain nucleation. It is also noted for negatively biased Pt/Co/Pt films that the domain nucleation in the descending branch of their hysteresis loops is denser than their ascending branch [38].

In this study, for the unbiased sample (IM0), a square-like hysteresis loop was obtained with symmetrical ascending and descending branches. The DW motion and domain nucleation are expected to be dominant mechanisms for this IM0 sample since these mechanisms are energetically more favorable for the single FM layers as Pt/Co/Pt thin films [17, 38]. In the biased IM10 and IM20 samples, the AFM layers strongly affect the reversal mechanism of the FM, causing DHLs. The reversal process involves a complicated domain structure for these samples. For IM10, one can say that both the domain nucleation and the DW motion play a significant role in both branches of its hysteresis loop with an apparent DHL due to the EB effect. On the other hand, the coherent and partial rotations are additionally involved in the increasing branch of the reversal process for IM20. This is due to the competition between the uniaxial and unidirectional anisotropies when the external magnetic field is applied [16].

The angle-dependent measurements in Fig. 4 demonstrated that the asymmetry seems to vanish with the change of the applied field angle from easy axis to hard axis of the magnetization. For the IM20 sample, its interface AFM spins have stronger upper IrMn volume as compared to IM10, therefore

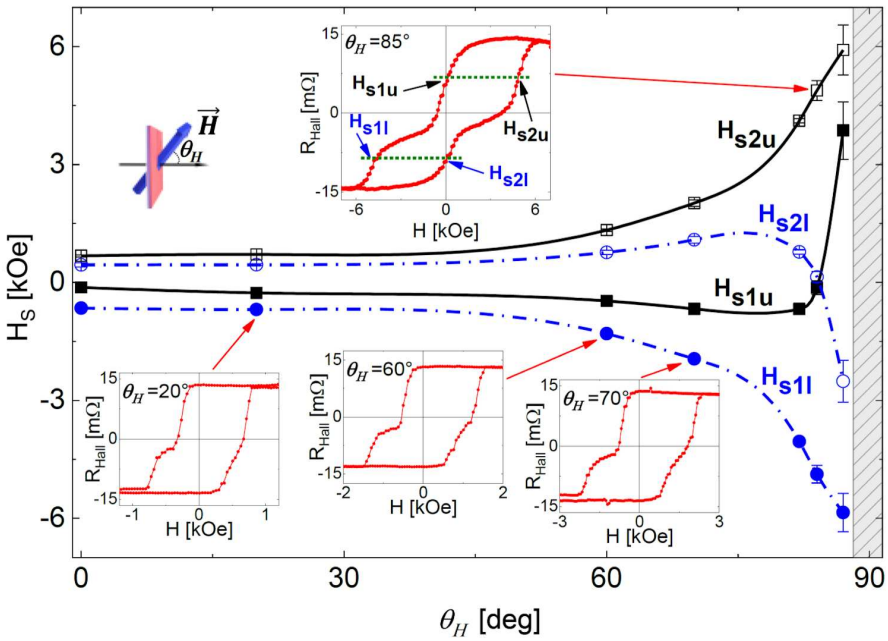

Fig. 4. The dependence of switching field values (H_{S1u}, H_{S2u}, H_{S1l} and H_{S2l}) with the polar angles. Upper inset ($\theta_H = 85°$) is provided to define the switching field symbols on a hysteresis loop. Switching field values are extracted from the hysteresis curves as approximate values during this approximation. Hysteresis curves are considered as DHLs where two separate lines passing through the approximate centers of upper and lower loops are drawn parallel to the x-axis (dotted green lines in the upper inset). The intersection points of the loop with the upper line are marked as H_{S1u} and H_{S2u}. Similarly, the intersection points of the loop with the lower line are marked as H_{S1l} and H_{S2l}. Error bars in the switching fields are defined by standard deviation of uncertainty since the data is approximate. Lower insets show the hysteresis measurements taken at 20°, 60°, and 70°. Lines in the figures are provided as guides to the eye. The gray hatched area around 90° indicates that no switching field data is extracted for this area from the hysteresis curves as the curves at these angles are arc-shaped.

its AFM domains become harder to mimic the FM domains. This is an overall effect where both the interface exchange decreases, and the thicker AFM layer prefers to order itself in a way closer to its bulk material. In fact, the AFM domain size (D_{AFM}) can be expressed as [14]:

$$D_{\mathrm{AFM}} = \frac{\pi^3}{2} t_{\mathrm{AFM}} \frac{J_{\mathrm{AFM}}}{J_{\mathrm{AFM-FM}}} \qquad (1)$$

by using the AFM thickness (t_{AFM}), the exchange coupling across the FM/AFM interface ($J_{\mathrm{AFM-FM}}$), and the AFM exchange constant (J_{AFM}) terms. It follows then that the increase in the AFM thickness will increase the AFM domain size and will affect the DW formation in the AFM. Microscopically, the formation of new DWs in the AFM causes asymmetry in the loops with changes in the nucleation centers since both the DW motion and the rotation are effective during the reversals [17].

In terms of anisotropy, the relative orientation of uniaxial, unidirectional, and other anisotropies on FM will change with increase of the AFM thickness. Misalignment between the competing anisotropies, and consequently the noncollinearity of FM and AFM easy axes, can be considered as the origin of the asymmetric ascending and descending branches in our measurement [21]. Since the Co layers in the studied samples are ultrathin, the asymmetry may also be associated with the inhomogeneities in the FM structure (which is also known as one of the intrinsic origins of asymmetric magnetization reversals [16]). The FM layers in the samples are ultrathin and interfaces have large values of roughness when compared to the FM layer thicknesses. However, this does not explain the relative symmetric situation in IM10 of this study, which has the same sample stack except for the thickness of its AFM layer. It can be assumed that the continuity of the ferromagnetic layer is supported by the induced magnetization of Pt at both sides due to their proximity effect. The samples with Pt layers constitute the case in which the ferromagnetic order within the layers should be taken into account to increase the effective ferromagnetic thickness [32].

Another potential cause of asymmetry to be considered is associated with the lateral inhomogeneity over the surface area of the sample, as a result of which the asymmetric shape emerges from the averaging in the measurement. However, if this was the case, the asymmetry should have also occurred in the measurement of IM10 or in the measurements of IM20 from different lateral regions. The MOKE measurements from different regions (the center or the sides, not shown in the article)

and the HE measurement resulted in similar data for the IM20 sample. Therefore, the mentioned inhomogeneity options cannot be expressed alone as the origin of asymmetric loops for our IM20 sample. But the possible inhomogeneity of the FM structure may provide additional contribution to the observed asymmetry, as reported in [16].

Apart from the loop asymmetry, the increase of the IrMn thickness seems to be the cause of a reduction in positive and negative values of EB in the hysteresis loops, as shown in Fig. 3a. Generally, the values of H_{EB} in FM/AFM bilayers are known to saturate with increasing AFM thickness after reaching a critical thickness value [12, 39]. However, the decrease in the H_{EB} values has been observed already in [14, 40]. In polycrystalline bilayers, in parallel, two different effects of the coupling of the FM spins to the AFM spins at the interface are usually observed: the hysteresis loop shift and the enhancement of coercive field values [40]. In our case, the values of the positive and negative loop shifts, which are the $\mathrm{H_{EB}}$ values for various domains, decrease for the IM20 sample. Remarkably, the coercive field values for the positive and negative parts of the loop seem to decrease as well. However, the value of the coercive field averaged over the left and right switching parts of the loops ($H_{C(\mathrm{av})}$) slightly increases. Since the hysteresis loops provided in Fig. 2 are normalized, a useful way to obtain the $H_{C(\mathrm{av})}$ is to calculate it through the total area under the hysteresis loops (we recall that the total area under the loop at the same time is a measure of the total magnetic anisotropy of this structure). The values of $H_{C(\mathrm{av})}$ are calculated as 420 ± 20 Oe for IM10 and 480 ± 20 Oe for IM20. This means that an overall effect of interface magnetic anisotropy increases as expected for the thicker film. Therefore, an increase in the IrMn thickness has caused an increase in $H_{C(\mathrm{av})}$ values despite an apparent decrease in the H_{EB} values. Hence, we attribute the above-mentioned reversal mechanism and the trend in the H_C values to a change in the density of the uncompensated spins at the interface with the enlargement of domain sizes. Obviously, we cannot exclude some effect of the interface roughness, which also contributes to the observed changes in parallel with the random field model of EB [41].

4. Conclusions

The emergence of DHLs in perpendicularly magnetized and exchange-biased Pt/Co/Pt/IrMn multilayers with varying antiferromagnetic layer thickness was analyzed by the magneto-optical Kerr and Hall effect techniques. For the sample without the IrMn layer, a symmetric square-like hysteresis loop was obtained. The growth of a 10 nm IrMn layer on top of the FM layer has resulted in the appearance of DHLs, while the measurement of the thickest sample with 20 nm IrMn has revealed asymmetric ascending and descending branches for its hysteresis loops. Changing the measurement angle of the external magnetic field from easy axis to hard axis has increased the symmetry of the DHLs. The observed DHLs were correlated with the bidomain nature of the sample due to the EB effect and the hysteresis loop asymmetries have been attributed to various magnetic reversal modes. It was shown that the appearance of both DHL and the hysteresis loop asymmetry in the samples is a complex phenomenon. This study also contributes to the understanding of the origin of this still debatable issue.

Further studies with additional new samples are currently being considered in order to determine the AFM thickness where the symmetrical DHL begins to transform into the asymmetric hysteresis. It is also of great interest to study the microscopic details of magnetization reversal in these structures by a MOKE microscopy, which is an effective way of visualization in the magnetization reversal process of the descending and ascending branches.

Acknowledgments

The author thanks Numan Akdoğan, Bulat Rameev, Muhammad Irfan, and Saim Spahi for their careful reading of the manuscript and their comments. The author would also like to acknowledge Bayram Kocaman for his support during the film deposition at the initial stage of this work. This work was supported by the Research Fund of the Gebze Technical University through the project No. BAP 2018-A105-43.

References

[1] W.H. Meiklejohn, C.P. Bean, *Phys. Rev.* **102**, 1413 (1956).

[2] M.E. Moskalev, E.V. Kudyukov, V.N. Lepalovskij, V.O. Vas'kovskiy, *IEEE Magn. Lett.* **10**, 1 (2019).

[3] Rui Wu, Mingzhu Xue, Tuhin Maity, Yuxuan Peng, Samir Kumar Giri, Guang Tian, J.L. MacManus-Driscoll, Jinbo Yang, *Phys. Rev. B* **101**, 014425 (2020).

[4] M. Ślęzak, P. Dróżdż, A. Kozioł-Rachwał, K. Matlak, J. Korecki, M. Zając, T. Ślęzak, *Acta Phys. Pol. A* **137**, 44 (2020).

[5] J.-J. Wang, W. Tang, H.-P. Xie, K. Wang, G.-H. Guo, *Acta Phys. Pol. A* **137**, 368 (2020).

[6] J.K. Murthy, P.S.A. Kumar, *Sci. Rep.* **7**, 6919 (2017).

[7] M. Vavra, M. Zentkova, M. Mihalik et al., *Acta Phys. Pol. A* **131**, 869 (2017).

[8] I. Dzhun, N. Chechenin, K. Chichay, V. Rodionova, *Acta Phys. Pol. A* **127**, 555 (2015).

[9] J. Dubowik, I. Gościańska, *Acta Phys. Pol. A* **127**, 147 (2015).

[10] S. Brück, J. Sort, V. Baltz, S. Surińach, J.S. Muńoz, B. Dieny, M.D. Baró, J. Nogués, *Adv. Mater.* **17**, 2978 (2005).

[11] X.J. Bai, X.X. Shi, C.D. Cao, M. Yang, W.X. Zhang, *J. Supercond. Nov. Magn.* **29**, 905 (2016).

[12] J.Y. Chen, N. Thiyagarajah, H.J. Xu, J.M.D. Coey, *Appl. Phys. Lett.* **104**, 152405 (2014).

[13] I.V. Roshchin, O. Petracic, R. Morales, Z.P. Li, X. Batlle, I.K. Schuller, *EPL* **71**, 297 (2005).

[14] J. Jia, Y. Chen, B. Wang, B. Han, Y. Wu, Y. Wang, J. Cao, *J. Phys. D Appl. Phys.* **52**, 065001 (2018).

[15] A.V. Svalov, O.A. Adanakova, A.N. Gorkovenko, V.N. Lepalovskij, E.A. Stepanova, N.V. Selezneva, V.O. Vas'kovskiy, *J. Magn. Magn. Mater.* **507**, 166839 (2020).

[16] Yang Liu, Shou-Guo Wang, Yang Li, Ning Li, Shuai Liu, Ning Chen, Ming-Hua Li, Guang-Hua Yu, *Phys. Rev. B* **84**, 104436 (2011).

[17] M. Gierlings, M.J. Prandolini, H. Fritzsche, M. Gruyters, D. Riegel, *Phys. Rev. B* **65**, 092407 (2002).

[18] S.P. Li, S. Kulkarni, S. Roy, *J. Appl. Phys.* **112**, 103918 (2012).

[19] J. McCord, R. Schäfer, R. Mattheis, K.-U. Barholz, *J. Appl. Phys.* **93**, 5491 (2003).

[20] S. Brems, D. Buntinx, K. Temst, C. Van Haesendonck, F. Radu, H. Zabel, *Phys. Rev. Lett.* **95**, 157202 (2005).

[21] Y. Huang, X. Wang, H. Wu et al., *J. Magn. Magn. Mater.* **494**, 165756 (2020).

[22] K. Theis-Bröhl, T. Schmitte, V. Leiner, H. Zabel, K. Rott, H. Brückl, J. McCord, *Phys. Rev. B* **67**, 184415 (2003).

[23] S.L. Gnatchenko, D.N. Merenkov, A.N. Bludov, V.V. Pishko, Y.A. Shakhayeva, M. Baran, R. Szymczak, V.A. Novosad, *J. Magn. Magn. Mater.* **307**, 263 (2006).

[24] F. Letellier, V. Baltz, L. Lechevallier, R. Lardé, J.F. Jacquot, B. Rodmacq, J.-M. Le Breton, B. Dieny, *J. Phys. D Appl. Phys.* **45**, 275001 (2012).

[25] C.Y. Tsai, J.-H. Hsu, K.F. Lin, *J. Appl. Phys.* **117**, 17D153 (2015).

[26] J. Sort, V. Baltz, F. Garcia, B. Rodmacq, B. Dieny, *Phys. Rev. B* **71**, 054411 (2005).

[27] W. Skowroński, M. Cecot, J. Kanak, et al., *Appl. Phys. Lett.* **109**, 062407 (2016).

[28] M. Öztürk, *J. Supercond. Nov. Magn.* **33**, 3097 (2020).

[29] J. Qiu, Z. Meng, Y. Yang, J.F. Ying, Q.J. Yap, G. Han, *AIP Adv.* **6**, 056123 (2016).

[30] S. Nakagawa, H. Yoshikawa, *J. Magn. Magn. Mater.* **287**, 193 (2005).

[31] I. Benguettat-El Mokhtari, A. Mourkas, P. Ntetsika, et al., *J. Appl. Phys.* **126**, 133902 (2019).

[32] L.G. Vivas, J. Rubín, A.I. Figueroa, et al., *Phys. Rev. B* **93**, 174410 (2016).

[33] S.D. Bader, *J. Magn. Magn. Mater.* **100**, 440 (1991).

[34] M. Öztürk, N. Akdoğan, *Turk. J. Phys.* **42**, 97 (2018).

[35] B. Kocaman, N. Akdoğan, *J. Magn. Magn. Mater.* **456**, 17 (2018).

[36] S. Chen, H. Zhao, G. Wang, Z. Zhang, B. Ma, Q.Y. Jin, *Thin Solid Films* **534**, 553 (2013).

[37] R.M. Rowan-Robinson, A.T. Hindmarch, D. Atkinson, *J. Appl. Phys.* **124**, 183901 (2018).

[38] F. Romanens, S. Pizzini, F. Yokaichiya et al., *Phys. Rev. B* **72**, 134410 (2005).

[39] R.A. Khan, H.T. Nembach, M. Ali, J.M. Shaw, C.H. Marrows, T.A. Moore, *Phys. Rev. B* **98**, 064413 (2018).

[40] G. Vinai, J. Moritz, S. Bandiera, I.L. Prejbeanu, B. Dieny, *J. Phys. D Appl. Phys.* **46**, 322001 (2013).

[41] A.P. Malozemoff, *Phys. Rev. B* **35**, 3679 (1987).